Nonequilibrium Green's function method: Büttiker probes for carrier generation and recombination

Kuang-Chung Wang[1], Yuanchen Chu[1], Daniel Valencia[1], Junzhe Geng[1,2], James Charles[1], Prasad Sarangapani[1], and Tillmann Kubis[1]

[1]School of Electrical and Computer Engineering, Purdue University, West Lafayette, IN 47906, USA
[2]Bloomberg, 731 Lexington Avenue, NY, 10022,USA

***Abstract*—The non-equilibrium Green function (NEGF) method is capable of nanodevice performance predictions including coherent and incoherent effects. To treat incoherent scattering, carrier generation and recombination is computationally very expensive. In this work, the numerically efficient Büttiker-probe model is expanded to cover recombination and generation effects in addition to various incoherent scattering processes. The capability of the new method to predict nanodevices is exemplified with quantum well III-N light-emitting diodes and anti-ambipolar 2D material heterojunctions.**

INTRODUCTION

Carriers recombination and generation enables devices such as solar cell [1] and light emitting diodes. An accurate device modeling is required for engineering and optimization. Drift-diffusion equation with the continuity equation [2] has served predicting carrier transport for device optimization. As optoelectronic and nano-electronic devices reach nanoscale and with the advent of novel 2D materials [3], [4], quantum effects play a more important role in the device performance and efficiency. The non-equilibrium Green's function (NEGF) method is a well known quantum transport method that can realistically simulate nanodevices including surface roughness and grain boundaries [5], [6], imperfections, phonon scattering [7], and carriers recombinations [8], [9]. However, even with approximations [7], the method is computationally expensive when incoherent scattering is handled in the self-consistent Born approximation. In this work, an extension of the numerically very efficient Büttiker-probe model is presented that tackles electron hole recombination in the NEGF framework avoiding the self-consistent Born approximation.

METHOD

Electrons and holes are represented with electronic Hamilton operators that are read-in from density function theory tools and transformed into maximally localized Wannier functions [3] for MoS_2/BP structure. For III-N material, the Hamiltonian is represented in a 20 band atomistic tight binding model [10].

The electrostatic potentials are determined in semi-classical/Poisson self-consistent calculations prior to the quantum transport solutions. Electron and hole transport is solved within the nonequilibrium Green's function method. Incoherent scattering on phonons as well as all recombination mechanisms, such as Auger, Shockley-Read-Hall and optical transitions are modeled with Büttiker probes. The Büttiker probe method [11], [12] introduces phase breaking centers in the device that allows for particle thermalization. In the presented method, electrons and holes are solved separately and iteratively coupled via the energy and particle exchange of Büttiker probes as shown in Fig. 1. Büttiker probe scattering strengths are for the time being solved within the heuristic ABC model [13], [9]. It is a common condition for single carrier type Büttiker probes that the net current at each probe ($I_{m,h}$ for hole current or $I_{m,e}$ for electron current) has to vanish to conserve the number of particles Ref. [12]. This condition determines the local Fermi levels of the electron or hole Büttiker probes. In the case of recombination (R) or carrier generation (G), this condition is altered to have net vanishing current for the sum of hole and electron current densities

$$\int I_{m,e}(E)dE = -\int I_{m,h}(E)dE = R_m(n_m, p_m) + G \quad (1)$$

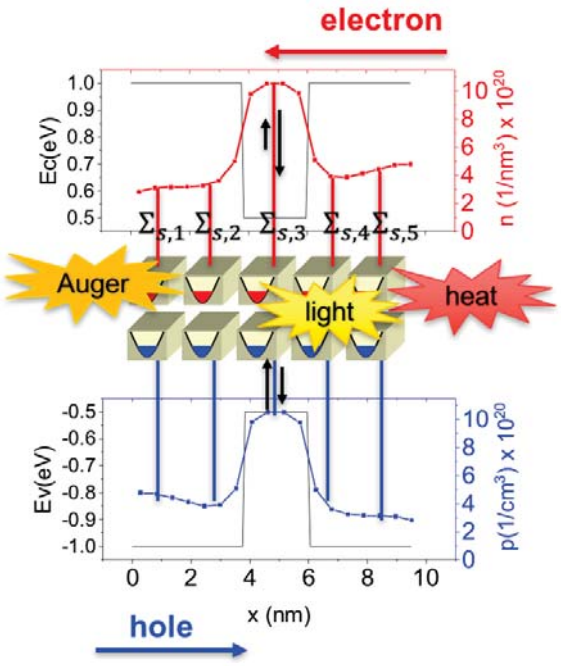

Fig. 1. A 10nm device with quantum well serves as a schematic of the Büttiker probe model. Probes are attached to electrons and holes with the probes covering Auger, Shockley-Read-Hall, and optical recombination processes.

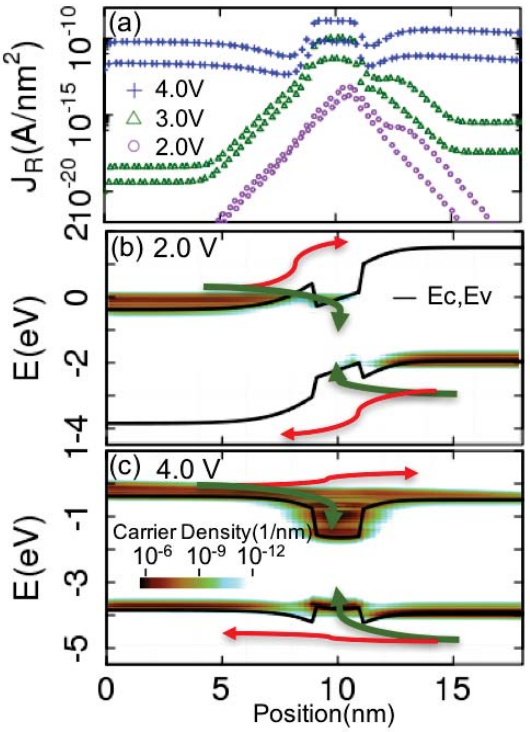

Fig. 2. (a) Spatially resolved recombination current for the device described in the main text for different voltages. Conduction and valence bands (lines) and contour plot of the energy and position resolved carrier density 2.0V (b) and 4.0V (c). Arrows indicate recombination current (green) and thermionic current (red).

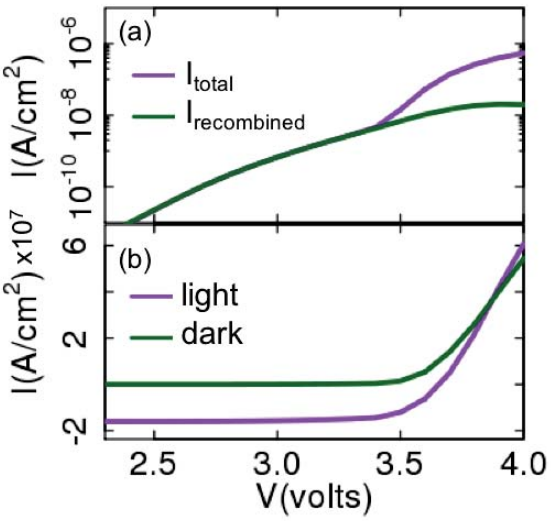

Fig. 3. Current voltage characteristics of the device in Fig. 2. (a) Without the generation of carriers, the contribution of recombination is assessed. A bias dependent balance between thermionic and recombination current is demonstrated where $I_{total} = I_{recombined} + I_{thermionic}$. (b) Total current is compared between device with and without carrier generation.

$$
\begin{aligned}
R_m(n_m, p_m) &= R_{SRH} + R_{recombination} + R_{Auger} \\
R_{SRH} &= \frac{n_m p_m - n_i^2}{\tau_N(p_m + p_1) + \tau_P(n_m + n_1)} \\
R_{recombination} &= B_m \cdot n_m p_m \\
R_{Auger} &= C_m \cdot (n_m^2 p_m + p_m^2 n_m)
\end{aligned}
\tag{2}
$$

Therefore, the Fermi-level vectors $E_{fn,m}$ for electrons and $E_{fp,m}$ for holes are adjusted to inject and extract carriers from the device to simulate generation and recombination processes, respectively, under the constraint of Eq. 1. The electron-hole generation and recombination probability is currently calculated heuristically with the ABC model [13] as listed in Eq. 2 assuming a constant generation rate [14], [14]. However, the Büttiker probe method is fully compatible with more sophisticated approaches.

All results of this work were generated with the multipurpose nanodevice simulation tool NEMO5 [15].

Results

NEGF results including incoherent scattering on phonons and the new recombination model for a 2nm wide intrinsic $In_{0.3}Ga_{0.7}N$ quantum well embedded in the center of a GaN pn junction ($10^{20}/cm^3$ doping density) biased in forward direction are shown in Figs. 2. Scattering is modeled with Büttiker probes of 10meV scattering strength independent of energy above the bandedge and decays exponentially into the bandgap with a decay length of 50meV. At low bias voltage, thermionic current is suppressed by a higher barrier and the total current is then mainly given by recombination (see Fig.2(a) and (b)). At high bias voltage, the recombination current increases due to increased carrier density in the quantum well. However, the effective barrier is much lower at higher voltages and the total current has an increasing thermionic contribution (see Figs. 2(a) and (c) as well as Fig. 3(a). The relevance of recombination is larger at lower voltages. The position and energy dependent occupation function is shown in Fig. 4(a). The variation of the distribution function with position highlights the non-equilibrium condition of the device. When a constant electron and hole generation rate of $2.4 \times 10^{-8}/cm^3$ in the quantum well region is assumed for the illuminated device, a shift in the IV curve is observed in Figs. 3(b). Simultaneously, the occupation function in Fig. 4(b) increases in the illuminated case as well.

Anti-ambipolar(AAP) performance is illustrated with a p-doped black phosphorus monolayer overlapping for 10nm with a monolayer of n doped MoS_2 system. Top and bottom gates are used to control the AAP performance (illustrated in Fig. 5(a)). Here, the new Büttiker probe model is applied on DFT-based electronic Hamiltonian operators in the maximally localized Wannier function representation. Shockley Read Hall (SRH) recombination rates are derived from the electron and hole density (shown in Fig. 5(b,c)) with Eq. 2. Note that in contrast to Figs. 2, a constant Büttiker probe strength is

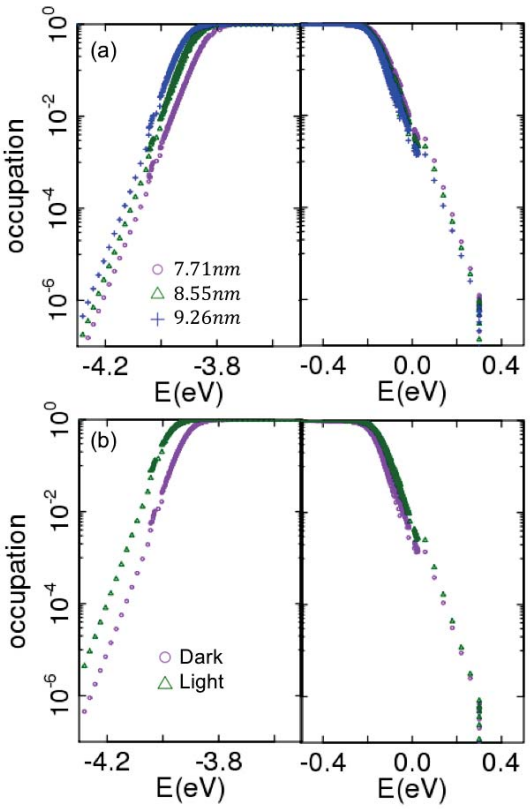

Fig. 4. (a) Occupation extracted from device shown in Fig. 2(c) for different positions.(b) Occupation is compared with device biased at 4.0V with and without carrier generation in the quantum well region. Occupation shifts more for the hole than the electron due to it's DOS distribution.

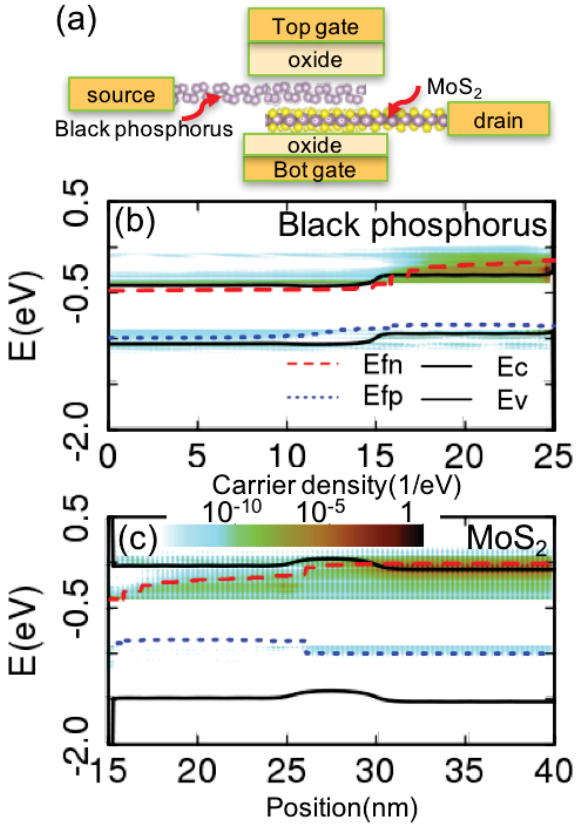

Fig. 5. (a) Schematic of the black phosphorus/MoS_2 heterojunction described in the main text. Conduction and valence bands (solid lines) as well as local Fermi levels (Efn for electrons, Efp for holes) superimposed with the contour plot of the position and energy resolved carrier density in black phosphorus (b) and MoS_2. The bottom gate is fixed at 0V. Left Fermi level is -1eV and right Fermi is 0eV. Carriers face a 10meV retarded Büttiker probe scattering self-energy.

assumed in Figs. 5, which results in a density of states that decays much slower into the gap than in the results of Fig. 2. The predicted AAP shown in Fig. 6 agrees qualitatively with experimental data [16]. The recombination, which causes the AAP behavior, is found to be tunable by the top and bottom gate.

Conclusion

Büttiker probes are a numerically efficient method to include incoherent scattering in nonequilibrium Green's function calculations. This work extends this method to handle carrier recombination and generation while carefully satisfying the continuity equation for electrons and holes. Compared to latest optoelectronic multi-domain implementation of the NEGF method [9], this method avoids the assumption some device areas are in equilibrium. Optoelectronic devices that are driven farer from equilibrium can be modeled in this way, while still limiting the numerical load far below common self-consistent Born approximations.

Acknowledgment

This work was supported in part by Semiconductor Research Corporation (SRC) and NSF EFRI-1433510. We also acknowledge the Rosen Center for Advanced Computing at Purdue University for the use of their computing resources and technical support. This research is part of the Blue Waters sustained-petascale computing project, which is supported by the National Science Foundation (award number ACI 1238993) and the state of Illinois. Blue Waters is a joint effort of the University of Illinois at Urbana-Champaign and its National Center for Supercomputing Applications.

References

[1] K.-c. Wang and Y.-r. Wu, "Transition Rate in the InGaN Quantum Dot Intermediate-Band Solar Cell," pp. 822–825, 2011.

[2] Y.-R. Wu, R. Shivaraman, K.-C. Wang, and J. S. Speck, "Analyzing the physical properties of InGaN multiple quantum well light emitting diodes from nano scale structure," *Applied Physics Letters*, vol. 101, no. 8, p. 083505, 2012. [Online]. Available: http://aip.scitation.org/doi/10.1063/1.4747532

[3] K. C. Wang, T. K. Stanev, D. Valencia, J. Charles, A. Henning, V. K. Sangwan, A. Lahiri, D. Mejia, P. Sarangapani, M. Povolotskyi, A. Afzalian, J. Maassen, G. Klimeck, M. C. Hersam, L. J. Lauhon, N. P. Stern, and T. Kubis, "Control of interlayer physics in 2H transition metal dichalcogenides," *Journal of Applied Physics*, vol. 122, no. 22, 2017.

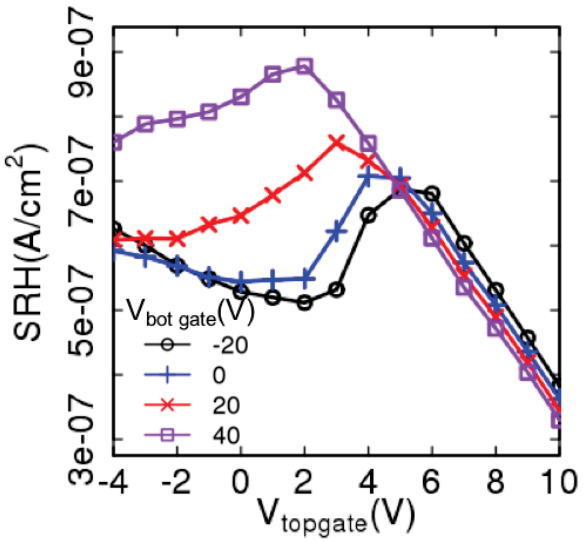

Fig. 6. SRH recombination current densities extracted form the NEGF calculations. A back gate tunable current is demonstrated with the peak value shifted towards negative $V_{topgate}$ as $V_{botgate}$ increases - in qualitative agreement with experiments [16].

[4] C.-y. Chen, T. A. Ameen, H. Ilatikhameneh, R. Rahman, G. Klimeck, and J. Appenzeller, "Channel thickness optimization for ultra thin and 2D chemically doped TFETs," pp. 1–6.

[5] D. Valencia, E. Wilson, P. Sarangapani, G. A. Valencia-Zapata, G. Klimeck, M. Povolotskyi, and Z. Jiang, "Grain boundary resistance in nanoscale copper interconnections," in *2016 International Conference on Simulation of Semiconductor Processes and Devices (SISPAD)*. IEEE, 2016, pp. 105–108.

[6] D. Valencia, E. Wilson, Z. Jiang, G. A. Valencia-Zapata, K.-C. Wang, G. Klimeck, and M. Povolotskyi, "Grain-boundary resistance in copper interconnects: From an atomistic model to a neural network," *Phys. Rev. Applied*, vol. 9, p. 044005, Apr 2018. [Online]. Available: https://link.aps.org/doi/10.1103/PhysRevApplied.9.044005

[7] J. Charles, P. Sarangapani, R. Golizadeh-Mojarad, R. Andrawis, D. Lemus, X. Guo, D. Mejia, J. E. Fonseca, M. Povolotskyi, T. Kubis, and G. Klimeck, "Incoherent transport in NEMO5: realistic and efficient scattering on phonons," *Journal of Computational Electronics*, vol. 15, no. 4, pp. 1123–1129, 2016.

[8] U. Aeberhard, "Theory and simulation of quantum photovoltaic devices based on the non-equilibrium Green's function formalism," *Journal of Computational Electronics*, vol. 10, no. 4, pp. 394–413, 2011.

[9] J. Geng, P. Sarangapani, K.-C. Wang, E. Nelson, B. Browne, C. Wordelman, J. Charles, Y. Chu, T. Kubis, and G. Klimeck, "Quantitative Multi-Scale, Multi-Physics Quantum Transport Modeling of GaN-Based Light Emitting Diodes," *Physica Status Solidi (a)*, vol. 1700662, p. 1700662, 2017. [Online]. Available: http://doi.wiley.com/10.1002/pssa.201700662

[10] ——, "Quantitative Multi-Scale, Multi-Physics Quantum Transport Modeling of GaN-Based Light Emitting Diodes," *Physica Status Solidi (a)*, vol. 1700662, p. 1700662, 2017. [Online]. Available: http://doi.wiley.com/10.1002/pssa.201700662

[11] M. P. Anantram, M. S. Lundstrom, and D. E. Nikonov, "Modeling of nanoscale devices," *Proceedings of the IEEE*, vol. 96, no. 9, pp. 1511–1550, 2008.

[12] R. Venugopal, M. Paulsson, S. Goasguen, S. Datta, and M. S. Lundstrom, "A simple quantum mechanical treatment of scattering in nanoscale transistors," *Journal of Applied Physics*, vol. 93, no. 9, pp. 5613–5625, 2003.

[13] J. Piprek, "Efficiency droop in nitride-based light-emitting diodes," *Physica Status Solidi (A) Applications and Materials Science*, vol. 207, no. 10, pp. 2217–2225, 2010.

[14] M. L. Inche Ibrahim, Z. Ahmad, and K. Sulaiman, "Analytical expression for the current-voltage characteristics of organic bulk heterojunction solar cells," *AIP Advances*, vol. 5, no. 2, 2015.

[15] S. Steiger, M. Povolotskyi, H. H. Park, T. Kubis, and G. Klimeck, "NEMO5: A parallel multiscale nanoelectronics modeling tool," *IEEE Transactions on Nanotechnology*, vol. 10, no. 6, pp. 1464–1474, 2011.

[16] V. K. Sangwan, M. E. Beck, A. Henning, J. Luo, H. Bergeron, J. Kang, I. Balla, H. Inbar, L. J. Lauhon, and M. C. Hersam, "Self-Aligned van der Waals Heterojunction Diodes and Transistors," *Nano Letters*, vol. 18, no. 2, pp. 1421–1427, 2018.